The 19th Conference of Mechanical Engineering Network of Thailand
19-21 October 2005, Phuket, Thailand

An Algorithm for Extracting Elastic-Plastic Properties of Indented Materials from Instrumented Sharp Indentation

Nuwong Chollacoop
National Metal and Materials Technology Center, 114 Paholyotin Rd, Pathumthani 12120
E-mail: nuwongc@mtec.or.th

Abstract

Over the past few decades, instrumented sharp indentation has extensively been utilized as a tool to extract mechanical properties of indented materials. The main advantages are the ease of specimen preparation, the ability to probe for localized properties and the non-destructive nature. Nonetheless, the direct indentation response requires further interpretation in order to arrive at mechanical properties. Simulation tool based on finite element method was adapted to construct a set of algorithms that allow for the prediction of indentation responses from the given elastic-plastic properties. Dimensional analysis was further applied in quest of another set of algorithms that allow for the extraction of elastic-plastic properties from the given indentation responses. Application and limitation of such algorithms are discussed.

Keywords: Instrumented indentation, Mechanical properties extraction, Finite element method, Dimensional analysis

1. Introduction

Instrumented sharp indentation has been a focus of intensive research and development over the past few decades [1-9, among many others] due to its novel capability to probe for localized mechanical properties of small volume structure (e.g. MEMS, electronic interconnects, thin film and nanocrystalline materials) without much complication in sample preparation. Advances in experimental instrumentation have enabled an accurate measurement of indentation load (P) and depth (h) as small as μN and nm, respectively. Simply saying, the indentation apparatus can be considered as an advanced version of typical hardness tester, where load and depth can be continuously monitored.

Figure 1 shows a schematic illustration of typical indentation response (P-h curve) of an elastic-plastic solid. As the sharp indenter advances into the material, the loading response follows Kick's law:

$$P = Ch^2 \qquad (1)$$

where P is the indentation load, C is the loading curvature, and h is the indentation depth. Upon unloading from a maximum load (P_m)/depth (h_m), the indented solid experiences elastic recovery, which is often used to correlate with elastic property via an initial unloading slope $\left.\frac{dP}{dh}\right|_{h_m}$. After complete unloading (P = 0), residual plastic deformation is remained in the solid at the indentation depth of h_r. The area underneath the loading curve is termed total work done by the indenter (W_t), which comprises of elastic recovery work (W_e) underneath the unloading portion and plastic permanent work (W_p) enclosed by the loading and unloading curves via $W_t = W_e + W_p$. Furthermore, $\frac{W_p}{W_t}$ or $\frac{h_r}{h_m}$ reflects a fraction of permanent deformation done by indenter in the solid. Thus, the indentation response is often characterized by these three parameters: loading curvature C, initial unloading slope S and plastic work ratio $\frac{W_p}{W_t}$ (or residual depth ratio $\frac{h_r}{h_m}$).

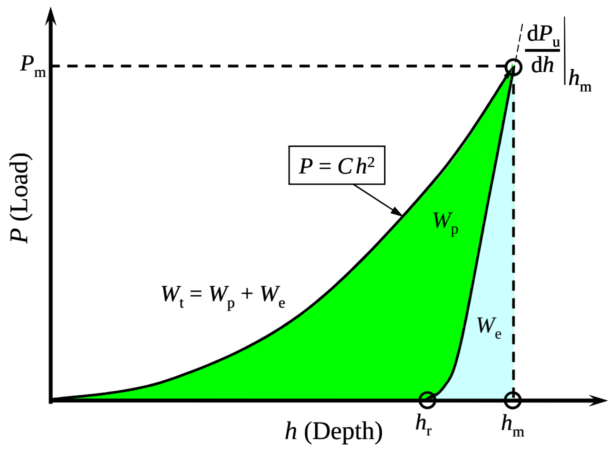

Figure 1. Schematic illustration of a typical P–h response of an elastic-plastic material to instrumented sharp indentation.

The main obstacle for making this indentation technique viable like any other mechanical testing methods (e.g. tensile test) is the robust algorithm to interpret indentation response, a load-vs-depth data. Such algorithm requires comprehensive understanding of the contact mechanics to analyze complicated stress state and deformation mechanism as a result of severe plasticity caused by sharp indenter tip penetrating into indented materials.

Early attempt to extract mechanical property from indentation data has dated back to the work of Tabor [1], where he has correlated hardness with the plastic flow of indented solid using the Vickers (four-sided pyramid) tip. His approximated relation of hardness being three times 8% flow stress, $H \approx 3\sigma_{0.08}$, is still used nowadays as a first-hand estimate from hardness result. Not until the work by Oliver and Pharr [3], who has further develop Doerner and Nix's result [4], the algorithms to extract elastic modulus (E) and hardness (H) from an initial unloading slope and the contact area have become readily available and routine to perform. However, such algorithms suffer an inaccurate prediction when there is a pile-up/sink-in of material flow against the face of the indenter tip. Moreover, the extraction of plastic properties (e.g. yield strength σ_y and work hardening exponent n) from indentation data is not done as routinely. Hence, the quest for a more accurate algorithm to extract elastic property and also some plastic properties is needed. The present study aims to establish such algorithm from the aforementioned indentation characteristics (C, S and $\frac{W_p}{W_t}$) by recourse to parametric finite element method and dimensional analysis [6].

2. Computational Methods

Indentation was simulated using general purpose finite element package ABAQUS [10]. Figure 2(a) shows an axisymmetric two-dimensional model setup, where a slant line representing a rigid conical indenter of an apex angle θ is placed on a block of elastic-plastic solid. The contact between rigid indenter and indented solid was assumed to be frictionless. As the severe plastic deformation is inevitable in the indentation process, non-linear geometry option in ABAQUS was used to emphasize the large deformation analysis. The axisymmetric model has been shown [6, 9] to give similar indentation response to the full three-dimensional model on the condition that the apex angle θ yields the same projected contact area as that of the actual tip geometry. For a commercially available Berkovich tip (three-sided pyramid) equppied in most indenter apparatus, the corresponding apex angle is 70.3° [6]. Figure 2b shows a detail mesh design of the region directly beneath the indenter tip. The semi-infinite block of the indented solid was modeled using 8,100 four-noded, bilinear axisymmetric quadrilateral elements, where a fine mesh near the contact region with gradually coarser mesh further away was carefully designed to ensure numerical accuracy. At the maximum load (P_m), at least 16 elements were in contact with the rigid indenter for each simulation performed here to ensure contact mechanic stability. The mesh designed was well-tested for numerical convergence and insensitivity to far-field boundary conditions. Details of the model setup were discussed elsewhere [6].

The constitutive relation of indented solid assumed linear elasticity ($\sigma = E\varepsilon$) and von Mises plasticity with power-law hardening, as shown in Fig. 3. For continuity at the yield point, the following relation is used to relate true stress and true strain in the plastic region, and also an input into FEM computation.

$$\sigma = \sigma_y \left(1 + \frac{E}{\sigma_y}\varepsilon_p\right)^n \qquad (2)$$

where σ is true stress, σ_y is yield strength, E is elastic modulus, ε_p is plastic true strain and n is strain hardening exponent.

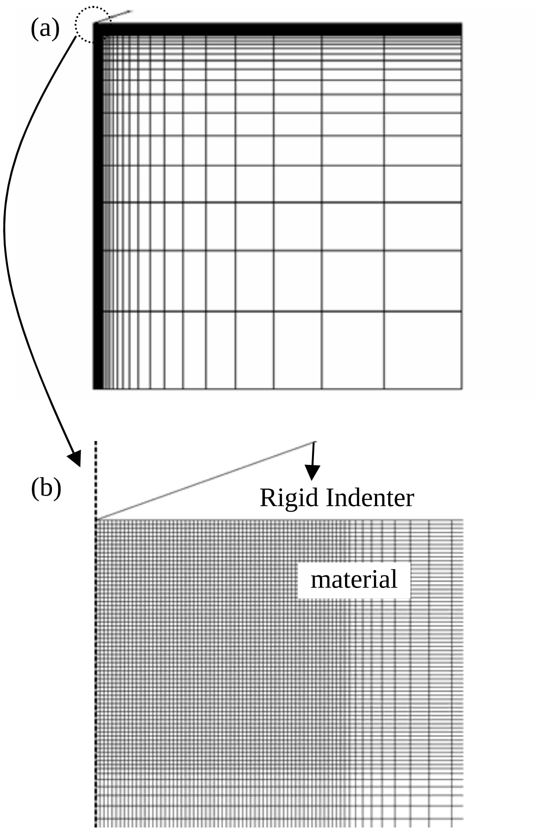

Figure 2. (a) Mesh design for axisymmetric finite element calculations with (b) a zoom in of the region in contact with the indenter tip.

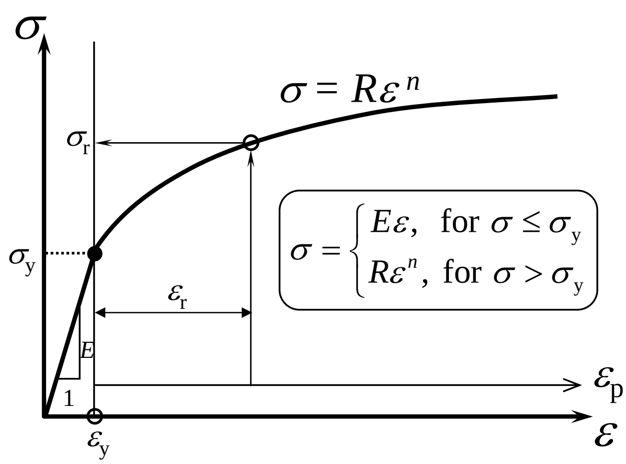

Figure 3. The power law elasto-plastic stress-strain behavior used in the current study.

A comprehensive parametric study, using various 76 combinations (see Table 1) of mechanical properties typically found in common engineering metals, was conducted. Each FEM *P-h* curve was obtained by monitoring the load felt by an indenter tip as it penetrated into the solid underneath in a displacement control manner. The FEM *P-h* curve also showed good agreement with experimental *P-h* curve performed in [6]. Dimensional analysis detailed elsewhere [6] was used to relate two parameter spaces: 76 sets of elastic-plastic properties (E, σ_y, n) as an input vs. 76 sets of *P-h* characteristics (C, $\left.\frac{\mathrm{d}P}{\mathrm{d}h}\right|_{h_m}$ and $\frac{W_p}{W_t}$) as a output. It is expected that there are many ways to establish such the relations, where *P-h* characteristics can be predicted from a given set of elastic-plastic properties—referred as forward analysis hereafter. On the other hand, the reverse analysis, which allows for an extraction of elastic-plastic properties from a given indentation response, must be considered simultaneously to achieve the more useful and significant results. Thus, only the most robust and accurate routes are presented here.

Table 1. Elasto-plastic parameters used in the present study. For each one of the 19 cases listed below, strain hardening exponent n is varied from 0, 0.1, 0.3 to 0.5, resulting a total of 76 different cases

E (GPa)	σ_y (MPa)	σ_y/E
10	30	0.003
10	100	0.01
10	300	0.03
50	200	0.004
50	600	0.012
50	1000	0.02
50	2000	0.04
90	500	0.005556
90	1500	0.016667
90	3000	0.033333
130	1000	0.007692
130	2000	0.015385
130	3000	0.023077
170	300	0.001765
170	1500	0.008824
170	3000	0.017647
210	300	0.001429
210	1800	0.008571
210	3000	0.014286

3. Results

In order to reflect non-ideally rigid tip used in experimental indentation, the elastic effect of indenter tip is compensated by using the reduced Young's modulus E^*:

$$E^* = \left[\frac{1-\nu^2}{E} + \frac{1-\nu_i^2}{E_i}\right]^{-1} \qquad (3)$$

where E_i is Young'd modulus of the indenter and ν_i is its Poisson's ratio. The major results of the dimensional analysis are illustrated here. First, the loading curvature from eq. (1) can be written as:

$$C = \frac{P}{h^2} = \sigma_r\,\Pi_1\left(\frac{E^*}{\sigma_r}, n\right) \rightarrow \frac{C}{\sigma_r} = \Pi_1\left(\frac{E^*}{\sigma_r}, n\right) \qquad (4)$$

where σ_r is representative stress at $\varepsilon_p = \varepsilon_r$ in eq. (2). By varying the value of representative strain ε_r for all 76 cases, Fig. 4 clearly shows that all points collapse into a 'single' curve when $\varepsilon_r = 0.033$ is used (see Appendix for explicit form of the equation). This significant finding suggests that there is a unique value of ε_r that allows eq. (4) to be n-independent. In other words, for any given *P-h* curve, if E^* is known, only the experimentally measurable C is required to predict the flow stress at 3.3% plastic strain, without knowing the hardening behavior of the material. This Π_1 function alone has enabled the extraction of one plastic property from the indentation response.

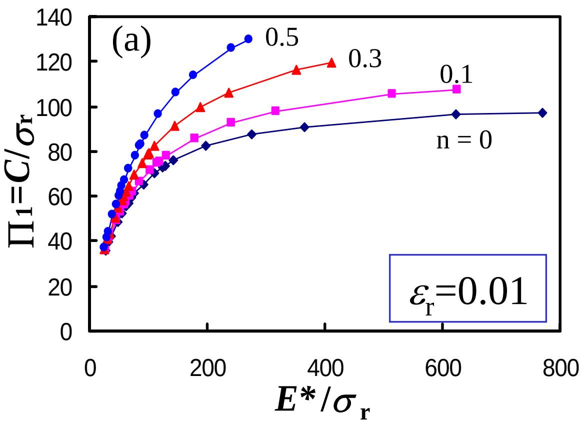

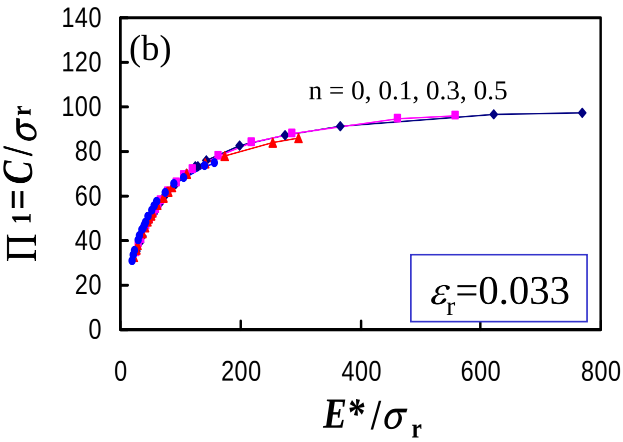

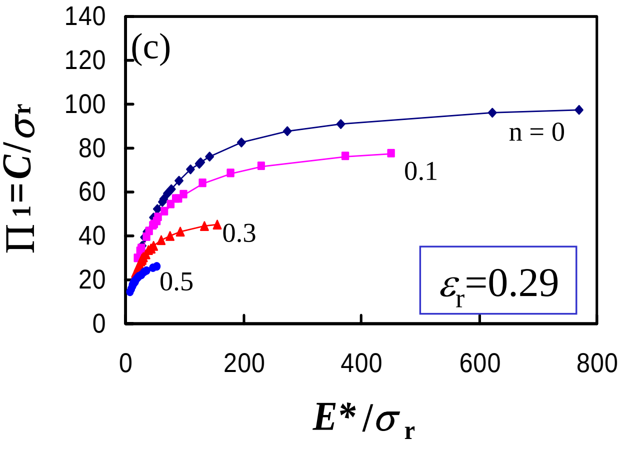

Figure 4. Dimensionless function Π_1 constructed using three different values of ε_r (i.e., $\varepsilon_p = 0.01$, 0.033 and 0.29) and the corresponding σ_r. For $\varepsilon_r < 0.033$, Π_1 increases with increasing n; for $\varepsilon_r > 0.033$, Π_1 decreases with increasing n. A representative plastic strain $\varepsilon_r = 0.033$ can be identified as a strain level which allows for the construction of Π_1 to be independent of strain hardening exponent n.

Apart from the Π_1 function, other dimensionless functions were constructed as follows:

$$\Pi_2\left(\frac{E^*}{\sigma_r}, n\right) = \frac{1}{E^* h_m} \left.\frac{dP_u}{dh}\right|_{h_m} \tag{5}$$

$$\Pi_3\left(\frac{\sigma_r}{E^*}, n\right) = \frac{h_r}{h_m} \tag{6}$$

$$\Pi_4\left(\frac{h_r}{h_m}\right) = \frac{p_{ave}}{E^*} \tag{7}$$

where p_{ave} is average contact pressure or approximately the hardness. Explicit functional forms of each dimensionless functions can be found in Appendix. It is often found in experimental P-h curve that a single value of residual depth h_r is extremely sensitive to the experimental error. Thus, the plastic work ratio $\frac{W_p}{W_t}$ is instead used to reduce the sensitivity and dependence upon a single point of complete unloading. Another dimensionless function was constructed as follows:

$$\Pi_5\left(\frac{h_r}{h_m}\right) = \frac{W_p}{W_t} \tag{8}$$

Following similar approach [3] to extract elastic modulus, another dimensionless function was constructed, with an improvement to account for pile-up/sink-in via a constant c^*.

$$\Pi_6 = \frac{1}{E^* \sqrt{A_m}} \left.\frac{dP_u}{dh}\right|_{h_m} = c^* \tag{9}$$

where A_m is contact area at maximum depth and c* is tip-dependent correction factor (= 1.1957, 1.2370 and 1.2105 for conical, Berkovich and Vickers tip, respectively.

Using eq. (2) -(9) to relate the parameter space of elastic-plastic properties in Table 1 to that of FEM P-h curves, the most robust pathway for forward and reverse analyses were constructed as in Figs. 5 and 6, respectively.

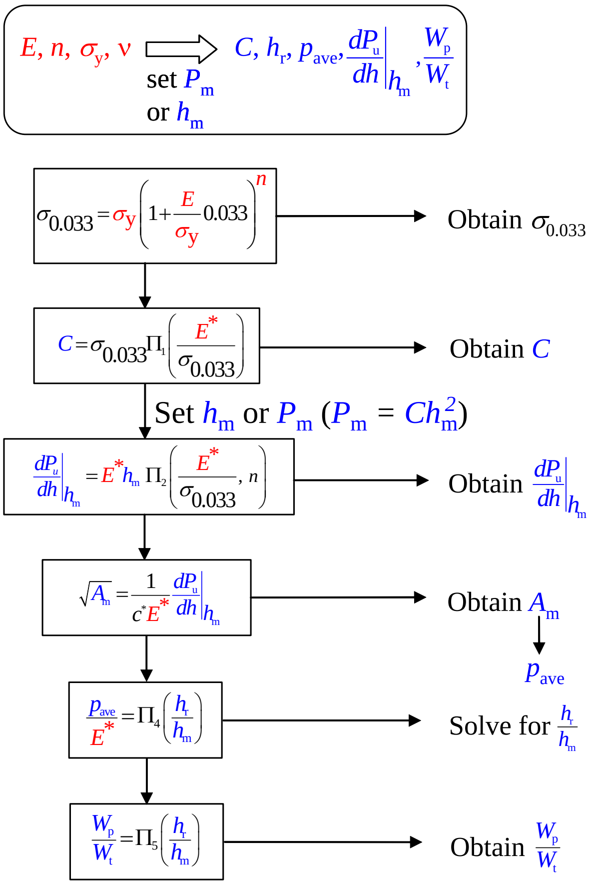

Figure 5. Forward analysis

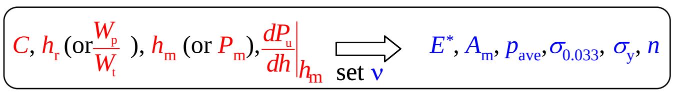

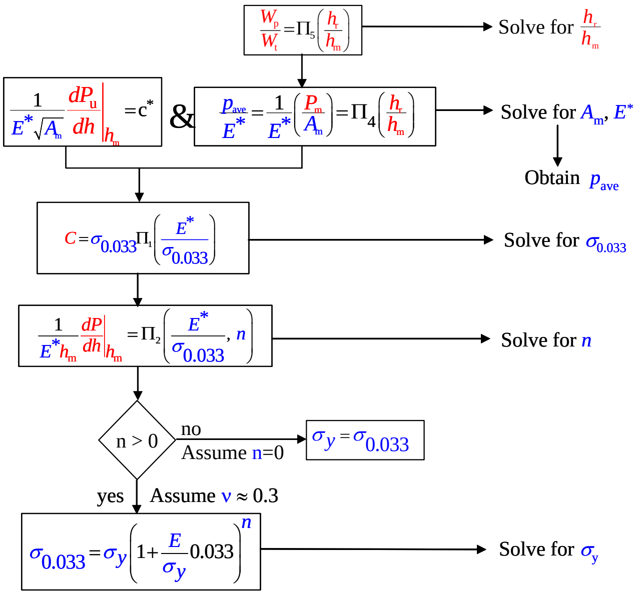

Figure 6. Reverse analysis

To assess intrinsic robustness of both forward and reverse algorithms without any uncontrolled experimental artifact, the sensitivity analysis was performed via FEM parametric study of small perturbation to the algorithm input. First consider forward algorithm, the perturbation of ±1, 2, 3, 4 and 5% deviation in any one input parameter (E^*, σ_y or n) of the 76 cases were analyzed with the forward algorithms. Over 2,200 cases were calculated, and the results were compared to the reference 76 cases. The results showed the maximum error of ±6% in the predicted results (C, $\left.\frac{dP}{dh}\right|_{h_m}$ and $\frac{W_p}{W_t}$). This small error was expected since the dimensionless functions, listed in an Appendix, were derived in the forward sense. The real sensitivity was then investigated in the reverse analysis, where any miniature error in numerical analysis may eventually build up in the final result. For reverse algorithm, the perturbation of ±1, 2, 3 and 4% deviation in any one input parameter (C, $\left.\frac{dP}{dh}\right|_{h_m}$ and $\frac{W_p}{W_t}$) of the 76 FEM P-h curves were calculated. Over 1,800 cases were calculated, and the results were compared to the reference 76 cases. Here, the general conclusion on the sensitivity cannot be drawn due to the largely different behaviors. Hence, statistical analysis was conducted to show the average trend with 99% confidence interval of the scattering, as shown in Fig. 7(a) - 7(d).

It is evident that E^* displays weak sensitivity to C and $\left.\frac{dP}{dh}\right|_{h_m}$, and moderate sensitivity to $\frac{W_p}{W_t}$. The σ_r displays weak sensitivity to C and $\left.\frac{dP}{dh}\right|_{h_m}$, and moderate sensitivity to $\frac{W_p}{W_t}$. The σ_y displays moderate to strong sensitivity to all three parameters. The p_{ave} displays weak sensitivity to C and $\left.\frac{dP}{dh}\right|_{h_m}$, and strong sensitivity to $\frac{W_p}{W_t}$.

The strong sensitivity of σ_y suggests that a need to take the averaged value from a number of indentation tests in order to reduce the error as the data scatter is random in nature

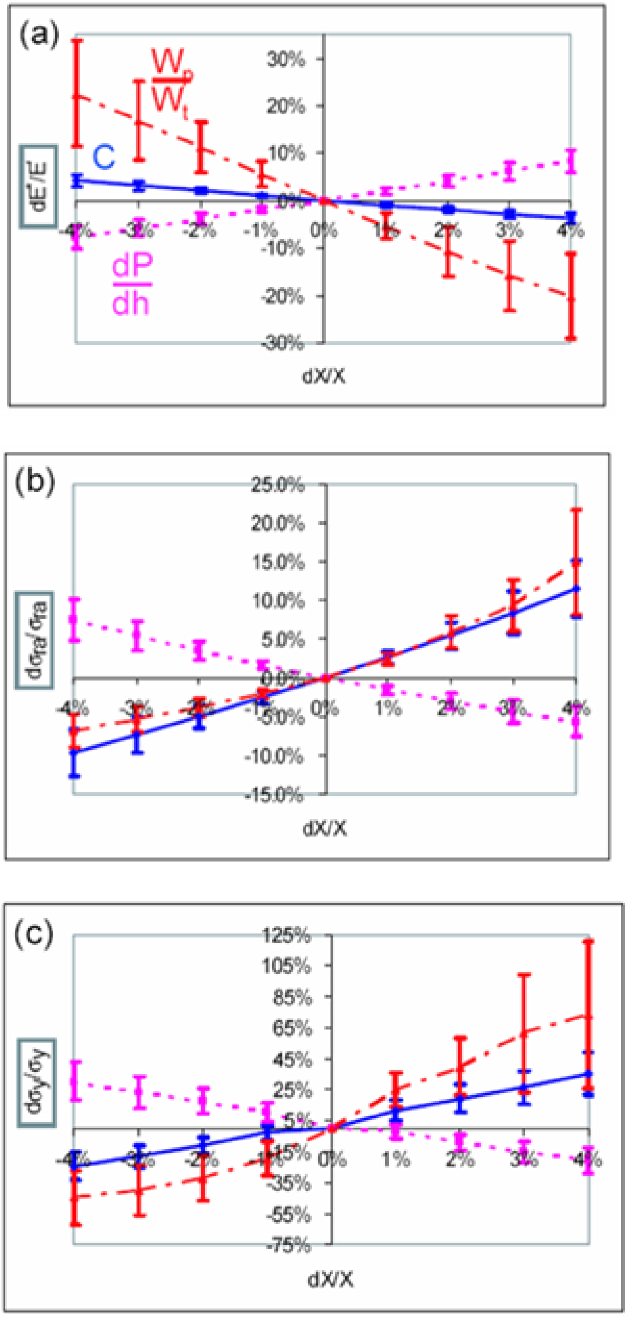

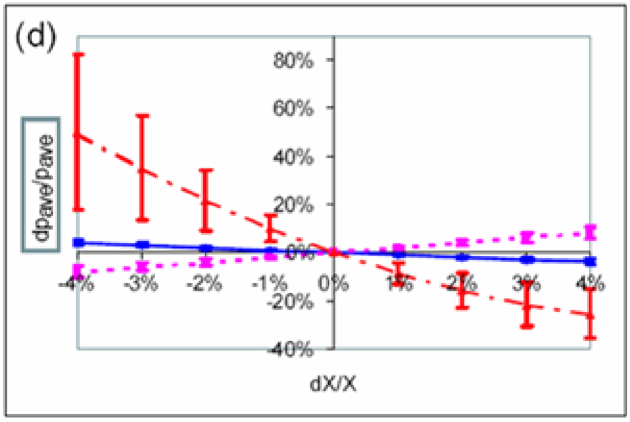

Figure 7. Sensitivity charts for reverse analysis showing the average variations in (a) E^*, (b) $\sigma_{0.033}$, (c) σ_y and (d) p_{ave} due to ±1, 2, 3 and 4% perturbation in C (solid line), $\left.\frac{dP}{dh}\right|_{h_m}$ (dotted line) and $\frac{W_p}{W_t}$ (dash-dotted line), with the error bar indicating 99% confidence interval.

4. Conclusion

The present study aims to apprehend the essence of mechanics involved in the indentation process by recourse to large deformation parametric finite element studies and dimensional analysis. The key results are as follows.

1. Using dimensional analysis, a set of new universal, dimensionless functions were constructed to characterize instrumented sharp indentation. From these functions and elastic-plastic finite element computations, solutions were formulated to relate indentation data to elastic-plastic properties.
2. For sharp indentation (Berkovich tip) of power law hardening pure metals and alloys, a representative strain ε_r was identified at 3.3%, which allows for the relationship among C, E^* and $\sigma_{0.033}$, without the knowledge of material's work hardening n.
3. Forward and reverse analysis algorithms were established based on the identified dimensionless functions. These algorithms allow for the calculation of the indentation response for a given set of properties, and also for extraction of some elastic-plastic properties from a given set of indentation data.
4. Comprehensive sensitivity analyses were carried out for both forward and reverse algorithms. Forward algorithm was found to be accurate and robust; a ±5% error in any input parameter results in less than ±6% in the predicted values of C, $\left.\frac{dP}{dh}\right|_{h_m}$ and $\frac{W_p}{W_t}$. On the other hand, reverse algorithm suffered greater sensitivity; E^*, $\sigma_{0.033}$ and p_{ave} displayed weak sensitivity to variations in C and $\left.\frac{dP}{dh}\right|_{h_m}$ but moderate to strong sensitivity to variations in $\frac{W_p}{W_t}$ while σ_y displayed moderate to strong sensitivity to variations in all three parameters (C, $\left.\frac{dP}{dh}\right|_{h_m}$ and $\frac{W_p}{W_t}$).
5. Although, plastic properties of materials extracted from instrumented indentation are very sensitive to even small variation in the P–h responses, the present computational study provides a mean to determine these plastic properties, which may not be easily obtainable by other means in small volume structures, and further provides an indication of the level of the sensitivity to experimental indentation data.

Acknowledgements

This research was supported by a subcontract to Massachusetts Institute of Technology (MIT) through the Center for Thermal Spray Research at Stony Brook, under the National Science Foundation Grant DMR-0080021, and by the Defense University Research Initiative on Nano-Technology (DURINT) on "Damage and Failure Resistant Nanostructured Materials and Interfacial Coatings" which is funded at MIT by the Office of Naval Research, Grant No. N00014-01-1-0808.

References

[1] D. Tabor, Hardness of Metals, Clarendon Press, Oxford, U.K., 1951.
[2] K.L. Johnson, Contact Mechanics, Cambridge University Press, London, U.K., 1985.
[3] W.C. Oliver and G.M. Pharr, J. Mater. Res., Vol. 7, 1992, pp. 1564
[4] M.F. Doerner and W.D. Nix, J. Mater. Res., Vol. 1, 1986, pp. 601.
[5] Special focus issue of J. Mater. Res., Vol. 19, No. 1, 2004.
[6] M. Dao, N. Chollacoop, K.J. van Vliet, T.A. Venkatesh and S. Suresh, Acta Mater., Vol 49, 2001, pp. 3899-3918.
[7] N. Chollacoop, M. Dao and S. Suresh, Acta Mater., Vol 51, 2003, pp. 3713-3729.
[8] N. Chollacoop and U. Ramamurty, Scripta Mater., Vol 53, 2005, pp. 247-251.
[9] Y.T. Cheng and C.M. Cheng, Mat. Sci. Eng. R, Vol 44, 2004, pp. 91-149.
[10] ABAQUS Version 6.1, 2000 Hibbitt, Karlsson and Sorensen, Inc., Pawtucket, USA

Appendix

In this appendix, six of the dimensionless functions, i.e. Π_1, Π_2, Π_3, Π_4, Π_5 and Π_6, are listed explicitly.

$$\Pi_1 = \frac{C}{\sigma_{0.033}} = -1.131\left[\ln\left(\frac{E^*}{\sigma_{0.033}}\right)\right]^3$$

$$+13.635\left[\ln\left(\frac{E^*}{\sigma_{0.033}}\right)\right]^2 - 30.594\left[\ln\left(\frac{E^*}{\sigma_{0.033}}\right)\right] + 29.267$$

$$\Pi_2\left(\frac{E^*}{\sigma_r}, n\right) = \frac{1}{E^* h_m}\left.\frac{dP_u}{dh}\right|_{h_m} =$$

$$\left(-1.406n^3 + 0.775n^2 + 0.158n - 0.0683\right)\left[\ln\left(\frac{E^*}{\sigma_{0.033}}\right)\right]^3$$

$$+\left(17.930n^3 - 9.221n^2 - 2.377n + 0.863\right)\left[\ln\left(\frac{E^*}{\sigma_{0.033}}\right)\right]^2$$

$$+\left(-79.997n^3 + 40.556n^2 + 9.002n - 2.545\right)\left[\ln\left(\frac{E^*}{\sigma_{0.033}}\right)\right]$$

$$+\left(122.651n^3 - 63.884n^2 - 9.589n + 6.200\right)$$

$$\Pi_3\left(\frac{\sigma_r}{E^*}, n\right) = \frac{h_r}{h_m} =$$

$$\left(0.0101n^2 + 0.00176n - 0.00408\right)\left[\ln\left(\frac{\sigma_{0.033}}{E*}\right)\right]^3$$

$$+\left(0.144n^2 + 0.0182n - 0.0882\right)\left[\ln\left(\frac{\sigma_{0.033}}{E*}\right)\right]^2$$

$$+\left(0.595n^2 + 0.0341n - 0.654\right)\left[\ln\left(\frac{\sigma_{0.033}}{E*}\right)\right]$$

$$+\left(0.582n^2 - 0.0885n - 0.673\right)$$

$$\Pi_4 = \frac{p_{ave}}{E^*} \approx 0.269\left(0.995 - \frac{h_r}{h_m}\right)^{1.114}$$

$$\Pi_5 = \frac{W_p}{W_t} =$$

$$1.612\left\{1.131 - 1.748^{\left[-1.493\left(\frac{h_r}{h_m}\right)^{2.535}\right]} - 0.0752\left(\frac{h_r}{h_m}\right)^{1.136}\right\}$$

$$\Pi_6 = \frac{1}{E^*\sqrt{A_m}}\left.\frac{dP_u}{dh}\right|_{h_m} = c^*$$